Threshold for Thermal Ionization of an Aluminum Surface by Pulsed Megagauss Magnetic Field

T. J. Awe,* B. S. Bauer, S. Fuelling, and R. E. Siemon

University of Nevada, Reno, 5625 Fox Avenue, Reno, Nevada 89506, USA

The first measurement of the threshold for thermal ionization of the surface of thick metal by pulsed magnetic field (B) is reported. *Thick* aluminum—with depth greater than the magnetic skin layer—was pulsed with $\partial B/\partial t$ from 30–80 MG/μs. Novel loads avoided *nonthermal* plasma (from electron avalanche, or energetic particles or photons from arcs). Thermal plasma forms from 6061-alloy aluminum when the surface magnetic field reaches 2.2 MG, in qualitative agreement with numerical simulation results by Garanin *et al.* [J. Appl. Mech. Tech. Phys. **46**, 153 (2005)].

An important question for both basic science and applications is what state of matter is created from a thick metal surface Ohmically heated by an intense current pulse. The question of the conductivity of a metal surface under conditions of pulsed megagauss (MG) magnetic field has been posed since at least 1959 [1], when fields above 10 MG were produced by magnetic flux compression. A challenge has been uncertainty as to the state of the metal: liquid, vapor, warm dense matter, plasma, or a mixture of these. While considerable data exist for volumetrically heated thin wires [2–5], data have not been available for surface-heated thick metal. Plasma formation from Ohmically heated thick metal surfaces is much less certain than for thin wires, even for an order-of-magnitude higher linear current density. This is due in part to the continued availability of fresh underlying cold metal, whose high conductivity reduces the surface electric field and Ohmic heating to values that may be marginal for plasma to form. Although numerical modeling can describe how plasma heats on a surface [6], computational results can vary widely; for a magnetic-field pulse that rises to several MG, calculated peak temperatures may vary by orders of magnitude, from 0.1 to 100 eV. It is challenging to accurately model the interplay of magnetic diffusion, hydrodynamics, radiative energy transfer, and evolving material properties (e.g., resistivity varies by more than 10 orders of magnitude). Numerical predictions are particularly sensitive to numerical algorithms, material properties models, and computational parameters. This impacts a wide variety of applications, including ultrahigh magnetic-field generators, magnetized target fusion [7], transmission lines [8,9], and magnetically accelerated flyer plates [10]. In this Letter, we report the first experimental measurement of the thermal ionization threshold of the surface of thick metal in response to a pulsed multi-MG magnetic field.

Studying if, when, where, and how thermal plasma is created by pulsed MG magnetic field, in the surface-heating regime, poses a significant experimental challenge. Ultrahigh magnetic fields have been generated by imploding a conducting shell (liner) around a magnetic flux, for example, using high explosives [11] or high current [12].

Liquid, vapor, warm dense matter, and/or plasma may form on the inner liner wall as the compressed field reaches MG level [13]. The experiment reported here made multi-MG field by directly pulsing a high current on a conducting rod. This configuration enhances diagnostic access and reduces shot cost, but introduces new challenges. First, current pulses of substantial magnitude and rise rate are required to ensure that the penetration depth of the magnetic field is much smaller than the rod radius, and that multi-MG field is developed on the rod surface. In consequence, nonthermal plasma can be created due to electric-field-driven electron avalanche or photoionization from arcing electrical contacts. To avoid this, novel load hardware was developed and shown to mitigate nonthermal plasma production. The hardware design and performance is described below, after the current pulse requirements.

The 2-TW Zebra generator [14] is a suitable driver for experiments which examine the changes of state that occur in the interaction of pulsed multi-MG magnetic field with a thick conducting surface. For much of the data reported here the maximum current averaged 990 kA with standard deviation $\sigma = 30$ kA, independent of the initial rod diameter. The Zebra current, $I(t)$, rose exponentially to 100 kA (with rise time $\tau = 13$ ns), and then linearly from 100 to 900 kA for 70 ns, with $dI/dt = 1.1 \times 10^{13}$ A/s, to a maximum current of 1.0 MA. The skin depth starts at 0.017 mm in cold Al, and grows to nearly 0.1 mm in hot, resistive Al. Zebra's parameters allow a range of D_0 around 1 mm to meet the surface-heating and high field requirements. Rod diameters have ranged from 2.00 to 0.50 mm with peak magnetic fields of 1.5 to 4 MG (corresponding to $\partial B/\partial t$ of 30 to 80 MG/μs) generated on the expanding surfaces. The observed consistency of the Zebra current waveform for modest changes in load-vacuum-chamber inductance (associated with changes in initial rod diameter) is supported by detailed modeling [15].

The experiment provides a meaningful comparison for one-dimensional (1D) MHD modeling. Novel load designs mitigate nonthermal plasma formation from contact arcing [16,17] or electron avalanche. The low inductance of the

load and large transmission line gap avoid nonthermal plasma formation from energetic particles or photons emitted from the transmission line or high-voltage insulator regions [18]. Because of the fast rise of the Zebra current pulse, rod surfaces exhibit (radially dependent) 1D behavior until plasma formation [19], with MHD instability observed only afterwards. Because of the importance of achieving thermal, uniform, and symmetric plasma formation, many different load geometries, contact configurations, and rod diameters were evaluated.

Load hardware was successfully designed to mitigate nonthermal plasma formation [20]. To avoid arcs, electrical connections were made at large diameter with buried, high-pressure metal-to-metal contacts. To avoid electric field enhancement, transitions to smaller radii were made slowly and smoothly. Three of the most commonly used load assemblies are depicted in Fig. 1. The simple straight-rod load [1(a)] uses gravitationally seated anode and cathode plates, and has small-diameter slip-fit rod to anode-cathode electrical contacts. The "barbell" and "hourglass" loads [1(b) and 1(c)] connect to the power flow channel with "knife-edge" coupling hardware, which compress a large-diameter stainless steel ring through the aluminum oxide layer on the surface of the anode and cathode plates, decreasing the local contact resistance and current density. Barbell loads are machined from 6-mm-diameter cylinders to allow medium-diameter connections to the anode and cathode. Hourglass loads contain no contact points near the straight central section of the load, as the entire load is machined from a single piece of 3-inch-diameter Al stock.

Simple electrical contacts [Fig. 1(a)] generate arcs and nonuniform heating, with possible plasma formation by ultraviolet irradiation on rod surfaces far from the location of the arc. The response of contacts was characterized with imaged photomultipliers and an intensified, gated CCD camera. For the anode and cathode contacts of simple straight-rod loads [Fig. 1(a)], arcing begins at low current,
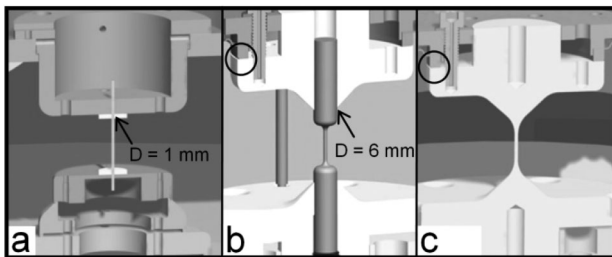

FIG. 1.   Three load assemblies: (a) Simple straight-rod load with small diameter contacts and gravitationally established electrical connections; (b) "Barbell" load with large diameter contacts and compressed knife-edge connections; and (c) "Hourglass" load machined from a single piece of Al with compressed knife-edge connections. Straight central-rod sections of barbell and hourglass loads are 7 mm long. Circles locate knife-edge penetration points.

and nonuniform plasma formation is observed on surfaces far from the current joints. In contrast, for barbell loads [Fig. 1(b)] no contact arcing is detected, and surface emission is much more spatially uniform. Hourglass loads [Fig. 1(c)] show surface emission uniformity similar to barbell loads.

Plasma is identified and characterized by a variety of independent measurements. Surface temperatures exceed 10 eV for surface magnetic fields (B_s) above 3 MG, as indicated by visible light radiometry. Multiply ionized Al is observed with time-resolved extreme ultraviolet (EUV) spectroscopy, and higher energy photons are detected with broadband EUV photodiodes. Plasma instabilities are recorded with gated imaging and laser shadowgraphy. The time-dependent value of B_s is determined by time-resolved measurements of the discharge current and the surface radius. The plasma formation time, temperature profiles, and surface expansion characteristics vary with the surface magnetic-field rise rate ($\partial B_s / \partial t$) and maximum ($B_{max}$), which increase when D_0 is decreased.

A lower bound on the surface temperature is obtained with visible light radiometry. The spectral radiation intensity escaping the rod is measured with a green-filtered linear diode array. The surface brightness temperature (T_{BB}) is then calculated by using the Planckian blackbody formula. Time-resolved spectroscopy (a visible light imaging spectrograph coupled to a streak camera) supports the blackbody assumption: a line-free continuum is observed from 1.00-mm-diameter rods. Simulations suggest the surface plasma is optically thick to visible radiation [21]. An optically thin body radiates less than a perfect blackbody; therefore, T_{BB} has low sensitivity to an optically thin corona.

Decreasing D_0 leads to earlier thermal plasma formation time (if plasma forms) and higher peak temperature. Peak T_{BB} occur near the time of peak current, and reach 36, 23, 20, 11, 1.3 and 0.7 eV for D_0 of 0.50, 0.80, 1.00, 1.25, 1.59, and 2.00 mm, respectively. For Al, multi-eV temperature clearly indicates plasma.

A second indicator of plasma was an EUV photon flux consistent with multi-eV temperatures, collected by photodiodes. Photodiodes filtered with 200 nm of Al or 100 nm of Si and 200 nm of Zr, are sensitive to photon energies from 16 to 73 eV, or 60 to 100 eV, respectively. EUV diode signals (Fig. 2) start when $T_{BB} \sim 2.0$ eV (from optical diodes), and signal amplitudes are consistent with the observed T_{BB} until the diodes saturate. The EUV flux was too low to be observed from 2.00-mm-diameter rods, consistent with a peak T_{BB} of only 0.7 eV (Fig. 2).

A third indicator of plasma was Al^{3+} and Al^{4+} line emission observed with time-resolved extreme ultraviolet (EUV) spectroscopy. EUV spectra (Fig. 3) in the band from 70 to 150 eV were obtained with a McPherson 310/G grazing incidence spectrometer equipped with a multistrip MCP. PrismSPECT, a commercial collisional-radiative
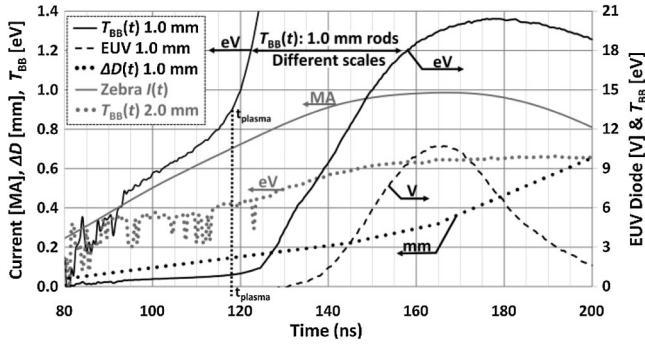
FIG. 2. $T_{BB}(t)$ [eV], Al-filtered EUV diodes [V], and change in rod diameter $\Delta D(t) = D(t) - D_0$ [mm], for 1.00 mm rods, and $T_{BB}(t)$ [eV] for 2.00 mm rods. Data are multishot averages. The average Zebra current is also plotted. Arrows (with units) designate the vertical scale for each curve. For $D_0 = 1.00$ mm, thermal plasma forms at $t_{plasma} = 118$ ns, as indicated by the abrupt increase in $\partial T_{BB}/\partial t$. For $D_0 = 2.00$ mm, plasma does not appear to form.

spectral analysis code, was used to estimate the plasma temperature (Fig. 3). The average ion charge and line ratios depend strongly upon temperature, and taking the ratio of line intensities results in an estimated peak plasma temperature of 15 ± 1 eV for 1.00-mm-diameter Al rods. Measurement uncertainty is much less than 1 eV, however, such precision is not realistic due to systematic uncertainty.

A fourth indicator of plasma was surface instabilities, whose development depends on the conductivity of the low density exploding material [22]. As indicated by time-gated imaging and laser shadowgraphy (Fig. 4), instabilities grow on the surface of rods with $D_0 \leq 1.25$ mm, and form earlier when D_0 is reduced.

A fifth possible indicator of plasma was a dramatic change at peak current of the surface radial expansion
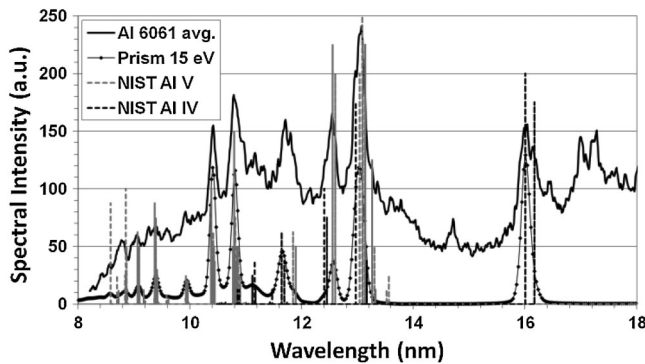

FIG. 3.   Average EUV spectrum during 6 ns near peak current from 1.00-mm-diameter Al-6061 barbell loads in knife-edge hardware. The data (thick line) are presented along with the wavelength and magnitude of Al^{3+} and Al^{4+} lines obtained from the NIST Atomic Spectra Database (vertical dashed lines), and a PrismSPECT-calculated spectrum for 15 eV temperature (thin line). PrismSPECT calculations assume a 1.0-μm-thick plasma layer with density 5×10^{-3} g/cm^3.

speed. Both 1.00 and 2.00-mm-diameter rods expand at a constant rate of 3 km/s until near peak current. Then as the current drops, the surface velocity for 1.00-mm-diameter rods exceeds 10 km/s, likely because of reduced magnetic pinching. In contrast, 2.00-mm-diameter rods remain at a constant 3 km/s velocity as the current drops.

The onset of thermal plasma is evident in the optical diode signals, as an abrupt increase in $\partial T_{BB}/\partial t$ when T_{BB} reaches 0.6 to 0.9 eV for $D_0 \leq 1.25$ mm (shown for 1.00 mm rods, Fig. 2). The observed plasma formation temperature is consistent with calculations of the conductivity of warm, dense Al at below one-tenth solid density [23]. This supports determining the plasma formation time and magnetic-field threshold ($B_{threshold}$) via the inflection in $T_{BB}(t)$.

Quite independent of D_0 (perhaps surprisingly), thermal plasma forms when B_s reaches $B_{threshold} = 2.2$ MG. By decreasing D_0, the rate of energy deposition via Ohmic heating $P_j(r, t) = \eta(r, t)[j(r, t)]^2 \approx \eta(r, t)\{I(t)/[\pi D_0 \Delta(t)]\}^2$ increases [where $\Delta(t)$ is the increasing thickness of the current-carrying skin layer]. Melting, vaporization, and plasma formation occur earlier, at lower current. For plasma to form, Ohmic heating must exceed energy losses associated with expansion, thermal conduction, and radiation. For each D_0, the material takes a different trajectory through $\rho - T$ space, with many orders of magnitude change in resistivity and heat capacity within the skin layer, yet the formation of plasma remains highly correlated with the value of B_s. The surface magnetic field is calculated using the radius observed in gated imaging and laser backlighting, and the load current deduced from differential magnetic (B-dot) probe measurements (Fig. 2). Rods with D_0 of 0.50, 0.64, 0.80, 1.00, and 1.25 mm form plasma when the B_s reaches 2.0, 2.1, 2.2, 2.3, and 2.2 MG, respectively. Plasma formation depends strongly upon B_s, but weakly upon magnetic-field rise rate ($\partial B_s/\partial t$ decreasing from 80 to 30 MG/μs) or upon nonplanar effects associated with small radius.

In conclusion, for $\partial B_s/\partial t$ of 30–80 MG/μs, thermal plasma forms from an Al 6061-alloy surface when B_s
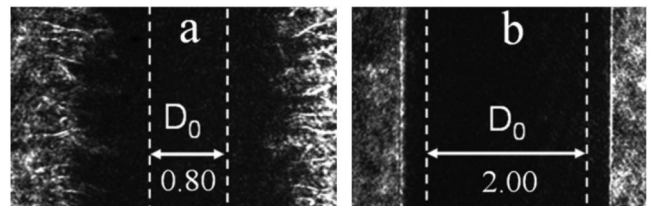

FIG. 4.   Laser shadowgrams (resolution 150 ps and 20 μm) for (a) 0.80-mm and (b) 2.00-mm-diameter rods, both at an instant near peak current (1 MA). Dashed lines indicate D_0. The 0.80 mm rod forms surface plasma at low current that is highly unstable. In contrast, the 2.00 mm rod forms no surface plasma, and within the resolution limits of the instrument, shows no instability formation even after significant radial expansion.

reaches 2.2 MG. The existence of a plasma formation
threshold at the few MG level is in qualitative agreement
with theoretical and numerical results [6]. The experiment
offers the first detailed study of the threshold for plasma
formation by pulsed magnetic fields on a thick Al surface.
Nonthermal plasma production has been effectively miti-
gated with specialized load hardware. For B_s below 2 MG,
sub-eV temperatures persist, and no evidence of plasma is
observed. Thermal plasma forms when T_{BB} reaches ap-
proximately 0.7 eV during the linear current rise, at which
point rapid surface heating is observed. For rods with $D_0 =$
1.00 mm, at peak current B_s is 3.0 MG, T_{BB} is 20 eV, and
Al^{3+} and Al^{4+} ions are observed in approximately equal
abundance. For a $\partial B_s / \partial t$ of 30–40 MG/μs, Al surfaces
expand at 3 km/s during the current rise. The detailed
measurements of phase, temperature, velocity, and ioniza-
tion state of a thick metal surface as a function of intense
pulsed magnetic field are informing radiation MHD mod-
eling and will facilitate the design and engineering of
practical devices.

*awetom@gmail.com
[1] C. M. Fowler, W. B. Garn, and R. S. Caird, J. Appl. Phys.
31, 588 (1960).
[2] *Exploding Wires*, edited by W. G. Chace and H. K. Moore
(Plenum, New York, 1968), Vol. 4.
[3] S. V. Lebedev and A. I. Savvatimskii, Sov. Phys. Usp. **27**,
749 (1984).
[4] M. G. Haines *et al.*, Phys. Plasmas **7**, 1672 (2000).
[5] D. A. Hammer and D. B. Sinars, Laser Part. Beams **19**, 377
(2001).
[6] S. F. Garanin *et al.*, J. Appl. Mech. Tech. Phys. **46**, 153
(2005).
[7] I. R. Lindemuth and R. E. Siemon, Am. J. Phys. **77**, 407
(2009).
[8] W. A. Stygar *et al.*, Phys. Rev. E **72**, 026404 (2005).
[9] S. A. Slutz, C. L. Olson, and P. Peterson, Phys. Plasmas **10**,
429 (2003).
[10] R. W. Lemke *et al.*, J. Appl. Phys. **98**, 073530 (2005).
[11] C. M. Fowler, Science **180**, 261 (1973).
[12] N. Miura *et al.*, Int. J. Mod. Phys. B **16**, 3379 (2002).
[13] P. J. Turchi, IEEE Trans. Plasma Sci. **28**, 1414 (2000).
[14] B. S. Bauer *et al.*, *Proceedings of the 4th International
Conference on Dense Z-Pinches, 1997* (AIP, Woodbury,
NY, 1999), Vol. 409, p. 153.
[15] A. S. Chuvatin *et al.*, *Proceedings of the 7th International
Conference on Dense Z-Pinches* (AIP, Melville, NY,
2009),Vol. 1088, p. 253.
[16] P. U. Duselis, J. A. Vaughan, and B. R. Kusse, Phys.
Plasmas **11**, 4025 (2004).
[17] T. W. L. Sanford *et al.*, Phys. Plasmas **12**, 122701 (2005).
[18] M. E. Cuneo, IEEE Trans. Dielectr. Electr. Insul. **6**, 469
(1999).
[19] R. E. Siemon *et al.*, J. Fusion Energy **27**, 235 (2008).
[20] S. Fuelling *et al.*, IEEE Trans. Plasma Sci. **36**, 62
(2008).
[21] S. Mazevet *et al.*, Phys. Rev. E **71**, 016409 (2005).
[22] M. A. Angelova *et al.*, IEEE Trans. Plasma Sci. **36**, 37
(2008).
[23] M. P. Desjarlais, J. D. Kress, and L. A. Collins, Phys. Rev.
E **66**, 025401(R) (2002).